Available online at www.sciencedirect.com

ScienceDirect

Procedia Manufacturing 26 (2018) 790–797

Procedia MANUFACTURING

www.elsevier.com/locate/procedia

46th SME North American Manufacturing Research Conference, NAMRC 46, Texas, USA

Force modeling for hybrid manufacturing

Michael Gomez[1], Jarred Heigel[2], and Tony Schmitz[1]*

[1]*UNC Charlotte, Mechanical Engineering and Engineering Science Department, 9201 University City Boulevard, Charlotte, NC 28223, USA*
[2]*National Institute of Standards and Technology, Production Systems Group, 100 Bureau Drive, Gaithersburg, MD 20899, USA*

* Corresponding author. Tel.: +1-704-687-5086.
E-mail address: tony.schmitz@uncc.edu

Abstract

This paper investigates the cutting forces during the machining of additively manufactured metals. Two pairs of workpieces were produced by powder bed direct metal selective laser sintering. These workpieces included a 17-4 stainless steel substrate (wrought) and a 17-4 stainless steel additively manufactured rib. After manufacture, one pair was annealed and the other was maintained in the as-produced state. Each was then machined to identify a cutting force model for the various material states. An instantaneous force, nonlinear optimization model was applied to determine the mechanistic cutting force coefficients. Due to the nonlinear dependence on the commanded feed per tooth, a power law fit was applied to the chip thickness-dependent cutting force coefficients. It was determined that there are only minor differences in the cutting force coefficients between the various material states. The strongest effect was annealing, which increased the mean coefficients in almost all cases, particularly for the additively manufactured bulk material.

Peer-review under responsibility of the scientific committee of the 4th International Conference on System-Integrated Intelligence.

Keywords: Additive manufacturing; machining; cutting force coefficients

1. Main text

Powder bed fusion (PBF) is an additive manufacturing (AM) technique that enables metal components with complex geometries to be produced. Increased surface roughness and increased dimensional uncertainty are disadvantages of AM as compared to computer numerically-controlled (CNC) machining [1]. To address these limitations, hybrid manufacturing combines additive and subtractive manufacturing strategies. This enables complex metal parts to be produced with the required surface finish and accuracy. An important consideration in hybrid manufacturing is the effect of the additive influence on material removal in the subtractive step.

2351-9789
Peer-review under responsibility of the scientific committee of the 4th International Conference on System-Integrated Intelligence.
10.1016/j.promfg.2018.07.096

To determine the influence of the additive step on the corresponding cutting forces, a mechanistic cutting force model is applied here to identify empirical coefficients that relate the required force for material removal to the commanded chip width and thickness. This paper characterizes these cutting force coefficients and explores the effects of the PBF process, as well as follow-on heat treating, on workpiece surface and material characteristics through a collaboration between UNC Charlotte and NIST*.

2. Additive workpieces

A total of four workpieces were used for the cutting tests. Each workpiece consisted of a wrought 17-4 stainless steel substrate (25 mm tall, 50 mm wide, 150 mm long) and a PBF-deposited rib (25 mm tall, 15 mm wide, 140 mm long). The PBF process parameters were held constant and repeated to create a second pair of workpieces. One set of workpieces was heat treated at 650 ºC for 1 hr, in an effort to relieve the residual stress generated by the PBF process, while the other set remained in the as-produced condition; see Figure 1.

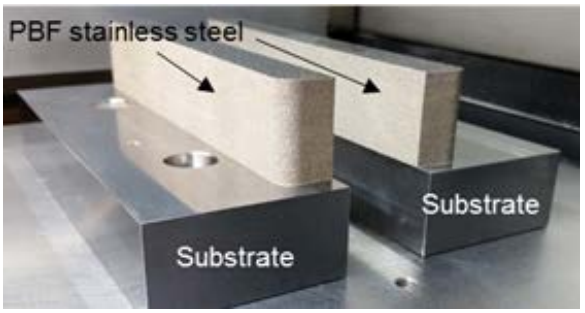

Fig. 1. One pair of as-produced workpieces mounted on the PBF build platform. Each workpiece has a PBF stainless steel rib (top section) and a wrought substrate (bottom section).

Three material regions of interest were identified: the wrought substrate, the AM surface material, and the AM bulk material. The wrought substrate served as a baseline material for which the AM material characteristics could be directly compared. The AM surface material was defined as the portion of the PBF-deposited material within 1 mm of the vertical faces of the PBF feature. The AM surface (shown by Figure 1) generated by the PBF build process exhibited the characteristic surface roughness. The AM bulk material was the remainder of the PBF feature and did not include the rough PBF surface.

Table 1. Overview of the AM workpieces and material regions of interest.

Workpiece	Material region	Heat treat	Effects
1, 3	Wrought substrate	No	As-produced baseline
1, 3	AM surface	No	Rough PBF surface
			Residual stress
1, 3	AM bulk	No	Residual stress
2, 4	Wrought substrate	Yes	Heat-treat baseline
2, 4	AM surface	Yes	Rough PBF surface
			Residual stress
2, 4	AM bulk	Yes	Residual stress

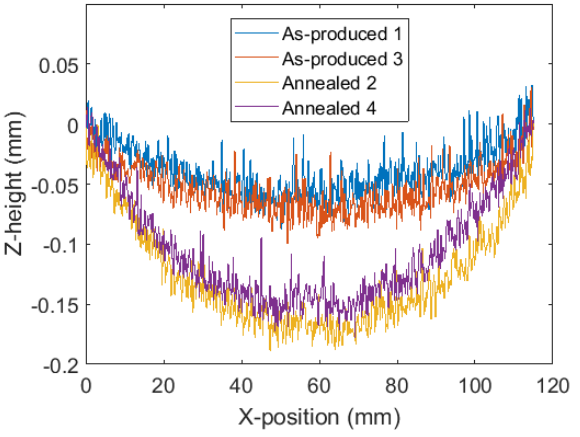

Fig. 2. Surface profile measurements along the top surface of the PBF stainless steel ribs.

* Certain commercial equipment, instruments, or materials are identified in this paper in order to specify the experimental procedure adequately. Such identification is not intended to imply recommendation or endorsement by the National Institute of Standards and Technology, nor is it intended to imply that the materials or equipment identified are necessarily the best available for the purpose. This material is declared a work of the U.S. Government and is not subject to copyright protection in the United States.

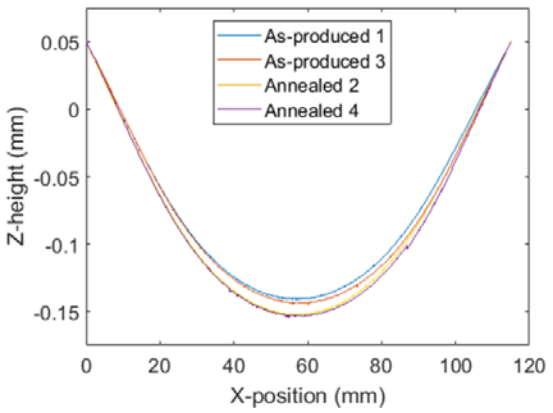

Fig. 3. Surface profile measurements along the bottom surface of the wrought substrate for each workpiece.

In order to characterize the geometric distortion in the AM workpieces, the top and bottom surfaces of the workpieces were measured with a MarSurf LD 260 stylus profilometer. A trace from a 120 mm section along the top surface of the PBF stainless steel substrates is provided in Figure 2. The high spatial frequency content is characteristic of the surface roughness from PBF processes. This is evident when comparing Figure 2 to Figure 3, which reports the same measurement performed on a 120 mm segment along the bottom of the wrought substrates for each pair of workpieces. From the results reported in Figures 2 and 3, the annealed workpieces experienced a greater amount of out-of-plane distortion.

3. Force modeling

There are a number of strategies available for cutting force modeling. In this paper, a mechanistic force model is applied to the milling process. The mechanistic force model is based on two underlying assumptions [2]: 1) the instantaneous cutting force is directly proportional to the chip thickness and width; and 2) the instantaneous cutting force is independent of other operating parameters. While these are acceptable assumptions for many applications, adjustments can be made to the force model to accommodate other process parameters [2, 3].

The cutting model applied in this study relates the uncut chip dimensions to the cutting force components using Eqs. 1-3 [2]:

$$F_t = k_t bh + k_{te} b \tag{1}$$

$$F_r = k_r bh + k_{re} b \tag{2}$$

$$F_a = k_a bh + k_{ae} b \tag{3}$$

where F_t, F_r, and F_a are the tangential, radial, and axial direction force components, respectively. The coefficients k_t, k_r, and k_a relate the force to chip area, where b is the axial depth of cut (chip width) and h is the instantaneous chip thickness. The edge coefficients k_{te}, k_{re}, and k_{ae} relate the force to the axial depth only and are associated with rubbing and non-cutting contact [2].

For this analysis, six different force models are established for the material regions of interest identified in Table 1. The empirical cutting force coefficients generated by the force model are then used to make a direct comparison between the as-produced and annealed PBF cases.

A nonlinear optimization algorithm was used to characterize the cutting force coefficients. The least-squares nonlinear optimization method [3] simulates the cutting forces over one cutter revolution using Eqs. 1-3. It then minimizes the differences between the simulated and measured cutting forces in the time domain. This optimization model takes the form of Eq. 4, where the x, y, and z force components are determined from a projection of the rotating force components (Eqs. 1-3) using the cutter rotation angle [3].

$$f(k_t, k_r, k_a, k_{te}, k_{re}, k_{ae}) = \sum \left\| \begin{Bmatrix} F_x \\ F_y \\ F_z \end{Bmatrix}_{simulated} - \begin{Bmatrix} F_x \\ F_y \\ F_z \end{Bmatrix}_{measured} \right\|^2 \tag{4}$$

4. Experimental setup

The cutting force coefficients were determined experimentally from a series of machining trials performed under stable, down-milling conditions. The axial and radial depths of cut were 3 mm and 1 mm, respectively. The spindle speed was held constant at 4000 rpm and the feed per tooth was varied. The details of the cutting tests are provided in Table 2.

The tests were carried out on a Haas TM-1 CNC milling machine with a maximum spindle speed of 4000 rpm. The workpieces were mounted on a three-axis force dynamometer (Kistler 9257B). Cutting tests were performed using a 19.05 mm diameter indexable

end mill with a single cutting insert attached (i.e., a single tooth tool). This configuration eliminated potential runout effects. Additionally, a new PVD-coated micro-grain carbide cutting insert (Sandvik Coromant 390R-070204E-MM S30T) was used for each test to mitigate the effects of tool wear. The machining setup for cutting force measurements is shown in Figure 4.

Table 2. Machining parameters used for cutting force measurements.

Feed per tooth [mm]	Spindle speed [rpm]	Milling direction	Axial depth of cut [mm]	Radial depth of cut [mm]
0.025-0.125	4000	Down	3	1

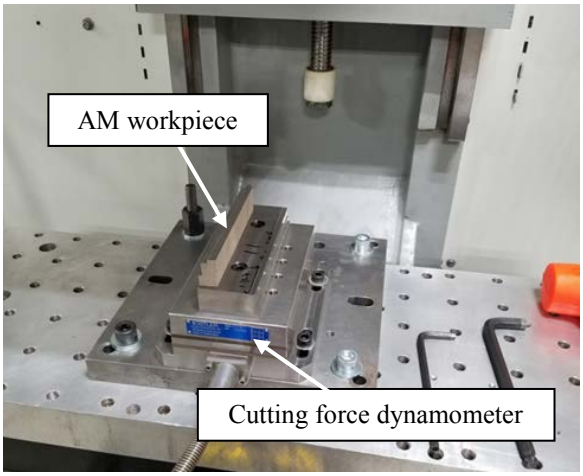

Fig. 4. Machining experimental setup.

Table 3. Cutting diameter measurement results.

Insert	Diameter difference [μm]
1	0
2	152
3	51
4	25
5	76
6	127
7	0
8	25
9	-25
10	102

Tool cutting diameter measurements were performed as each insert was replaced between tests. The results are displayed in Table 3, where the measurements were performed in the machine spindle using a Mitutoyo dial indicator and a Noga dial gage holder. It was concluded that this effect could be neglected in the subsequent force modeling.

The cutting force measurements were repeated two times for workpieces 1 and 2 and three times for workpieces 3 and 4 in order to establish a statistical mean and confidence intervals for the cutting force coefficients between tool and workpiece combinations.

5. Experimental results

In this section experimental results are presented. The cutting force coefficients calculated with the nonlinear optimization method over a range of feed per tooth values are compared for the different material states. Figures 5 and 6 show the mean values for tangential and radial cutting force coefficients at the commanded feed per tooth values including 95% confidence intervals for the repeated tests. There does not appear to be an appreciable difference between the pair of as-produced workpieces.

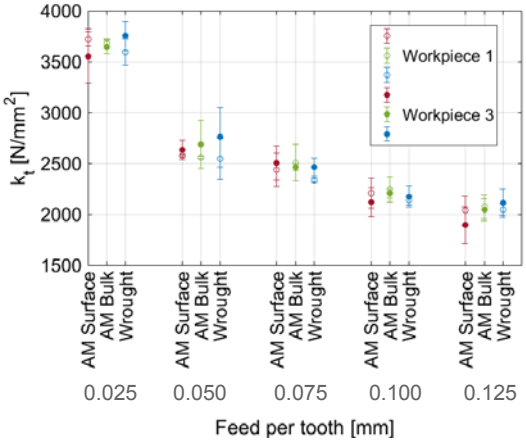

Fig. 5. Tangential cutting force coefficient mean values and 95% confidence intervals for the pair of as-produced workpieces.

Next, repeatability tests were carried out for the pair of annealed workpieces. The tangential and radial cutting force coefficients are provided in Figures 7 and 8, respectively. Once again, there is no significant difference between the tangential cutting force coefficients between the two workpieces. While the

confidence intervals for the radial cutting force coefficients do not overlap in every instance, there is a minimal observable difference between the material regions of interest.

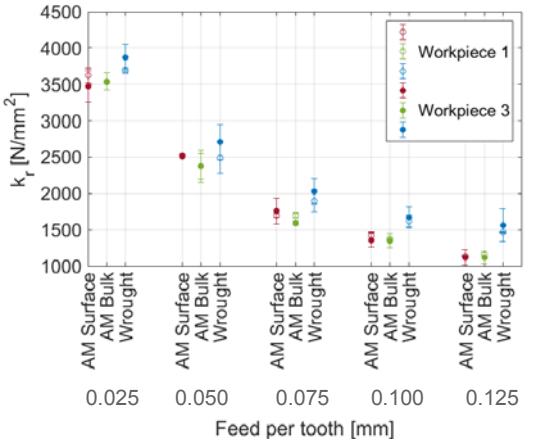

Fig. 6. Radial cutting force coefficient mean values and 95% confidence intervals for the pair of as-produced workpieces.

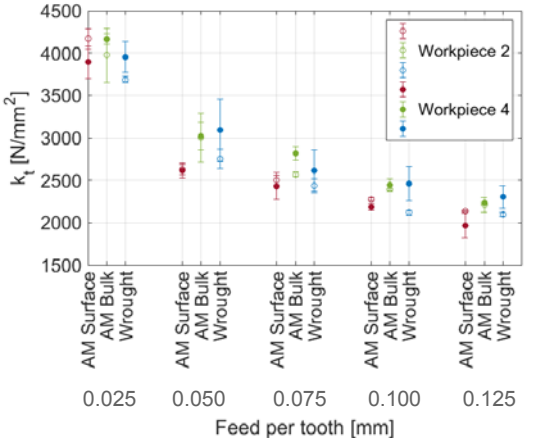

Fig. 7. Tangential cutting force coefficient mean values and 95% confidence intervals for the pair of annealed workpieces.

The results of the repeatability tests displayed in Figures 4-8 for the as-produced and annealed workpieces were next grouped for direct comparison. A total of six cutting force models for the material regions of interest are established. The results are presented in Figures 9 and 10. In nearly every instance, annealing increases the mean values in both the tangential and radial cutting force coefficients. The AM bulk material exhibits the most notable change in cutting force coefficients.

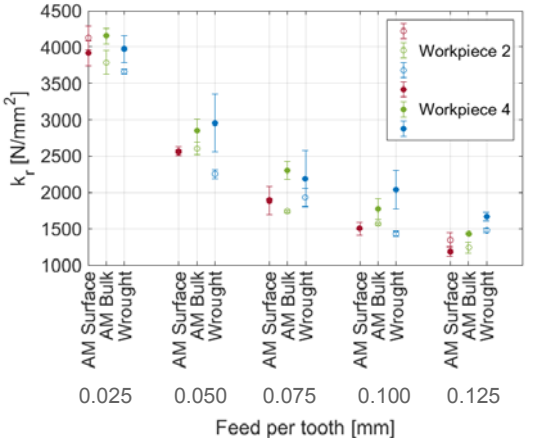

Fig. 8. Radial cutting force coefficient mean values and 95% confidence intervals for the pair of annealed workpieces.

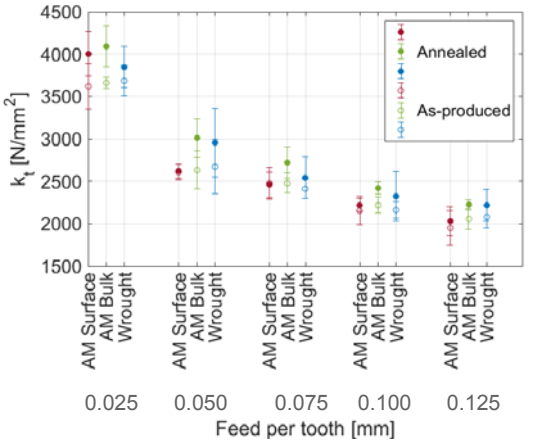

Fig. 9. Comparison of the tangential cutting force coefficients for the as-produced and annealed workpieces. The error bars identify 95% confidence intervals about the mean.

6. Power law fit

It is evident in Figures 9 and 10 that both the tangential and radial cutting force coefficients decrease with increasing feed per tooth (chip thickness). This results in a nonlinear relationship between the cutting force coefficients and feed per tooth [2]. This phenomena occurs when the chip thickness approaches the size of the cutting edge radius [3-4]. As the commanded feed per tooth

approaches the same order of magnitude as the cutting radius for the milling insert, the effective rake angle becomes negative. This negative rake angle serves to increase the cutting force coefficients.

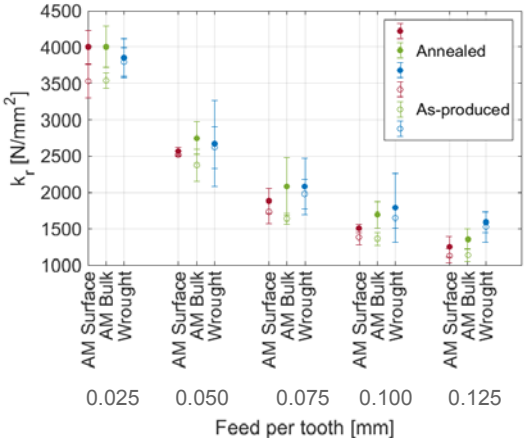

Fig. 10. Comparison of the radial cutting force coefficients for the as-produced and annealed workpieces. The error bars identify 95% confidence intervals about the mean.

A cutting insert was sectioned using wire electrical discharge machining (WEDM) to expose the cutting radius. The sectioned insert was then placed in a scanning electron microscope (SEM) to obtain an approximate cutting edge radius of 24.7 µm. An SEM image is displayed in Figure 11.

Based on Figures 9-11, the cutting force model was modified to account for the edge radius effect. In this case, a power law fit can be applied [6]:

$$F_t = A_t b h^{1-p_t} \tag{5}$$

$$F_r = A_r b h^{1-p_r} \tag{6}$$

$$F_a = A_a b h^{1-p_a} \tag{7}$$

where there is a power law relationship on the chip thickness through the p coefficients. The A and p coefficients are identified by a nonlinear least squares fit to the feed-dependent cutting force coefficients obtained from the nonlinear least squares optimization. Equations 8-10 define the relationship between the original, feed dependent nonlinear optimization model cutting force coefficients and the new A and p coefficients:

$$k_t = A_t f_t^{-p_t} \tag{8}$$

$$k_r = A_r f_t^{-p_r} \tag{9}$$

$$k_a = A_a f_t^{-p_a} \tag{10}$$

where k_t, k_r, and k_a, are the cutting force coefficients obtained from the nonlinear optimization model, A_t, A_r, and, A_a are the new coefficients obtained from the power law fit and p_t, p_r, and p_a are positive dimensionless constants with a value less than one.

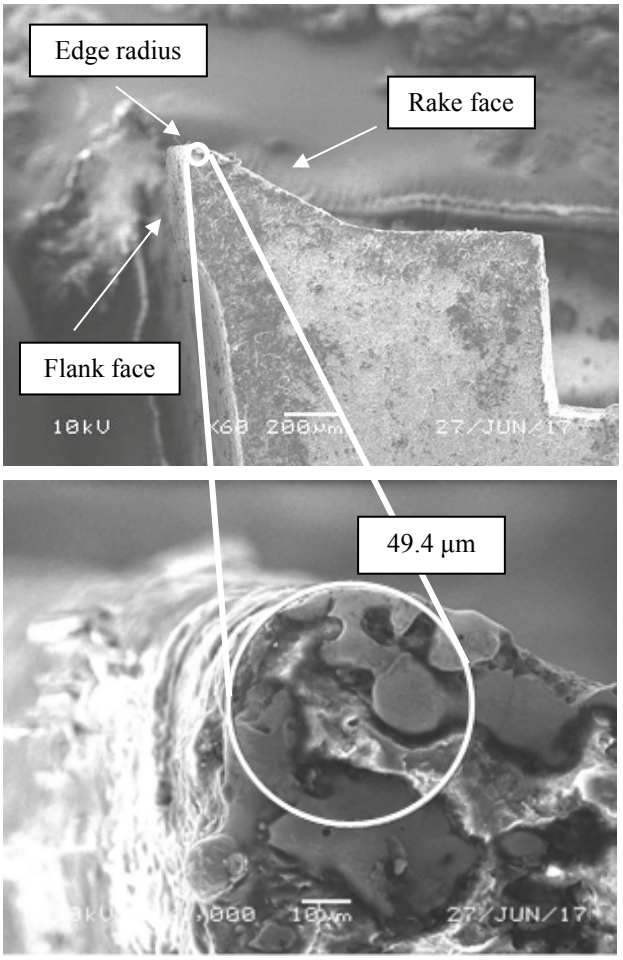

Fig. 11. SEM image of the sectioned cutting insert (top) and magnified SEM image of the cutting edge radius (bottom).

To determine the uncertainty in the power law fit, a Monte Carlo simulation was completed in which a random value was generated from normal distributions defined by the mean values and uncertainties from the cutting force coefficients. At each simulation iteration, the power law was fit to the sampled cutting force coefficients to determine the A and p fitting parameters. After 1×10^4 iterations, the mean and

standard deviation in the distribution of fit parameters was calculated. The results of this exercise are displayed in Tables 4 and 5, where the uncertainties correspond to the Monte Carlo simulation standard deviations.

Table 4. Power law coefficients generated from the Monte Carlo simulation for the as-produced workpieces.

As-produced material region	A_t [N/mm^3]	p_t	A_r [N/mm^3]	p_r
AM surface	911.9 ±138.6	0.3734 ±0.053	315.8 ±42.2	0.6627 ±0.046
AM bulk	964.4 ±68.1	0.3574 ±0.021	284.9 ±26.7	0.6872 ±0.028
Wrought	925.8 ±94.4	0.3716 ±0.036	451.0 ±71.0	0.5819 ±0.049

Table 5. Power law coefficients generated from the Monte Carlo simulation for the annealed workpieces.

Annealed material region	A_t [N/mm^3]	p_t	A_r [N/mm^3]	p_r
AM surface	804.9 ±105.3	0.4297 ±0.047	308.9 ±40.6	0.6984 ±0.045
AM bulk	1012.6 ±102.2	0.3773 ±0.038	407.8 ±79.6	0.6277 ±0.062
Wrought	1039.3 ±161.3	0.3562 ±0.051	519.8 ±132.8	0.5520 ±0.077

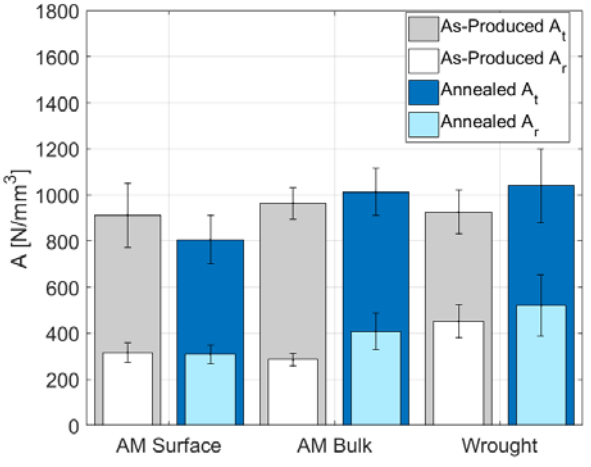

Fig. 12. Mean values and standard deviations of the coefficient A for as-produced and annealed states grouped by regions of interest.

The power law fit consolidates the feed-dependent specific cutting force coefficients to a pair of fit parameters for each material region. Furthermore, by using the fit parameters and Eqs. 8-10, the cutting force coefficient can be estimated based on the selection of the commanded feed per tooth. A graphical representation of the information in Tables 4-5 is displayed in Figures 12 and 13.

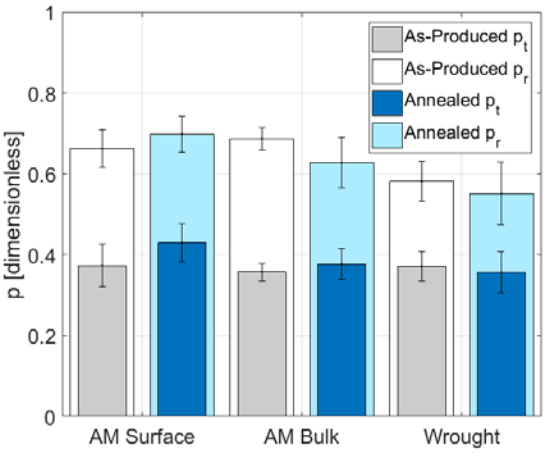

Fig. 13. Mean values and standard deviations of the coefficient p for as-produced and annealed states grouped by regions of interest.

7. Conclusions

The purpose of this project was to investigate the cutting forces generated during the machining of additively manufactured metals. Two conditions were considered: as-produced and annealed. In both material conditions, there were various material states of interest and, in each case, an instantaneous force nonlinear optimization method was used determine the cutting force coefficients.

The results showed only minor differences in the coefficients between the various material states. The most significant effect was annealing which increased the mean cutting force coefficients in nearly all instances.

A nonlinear trend of decreasing cutting force coefficients as a function of increasing feed per tooth was identified. Therefore, a power law fit was applied which incorporated the effect of the change in rake angle at low feed per tooth values. New power law fit coefficients were calculated which, again, did not

exhibit significant difference between the various material states.

To continue this research effort, a tool wear study will be carried out to investigate the possible changes in tool life when machining the different material regions of interest. Additionally, surface profile measurements will be completed to establish the change in surface finish as the tool wear progresses. Finally, AM samples will be polished and etched to investigate the possible change in grain structure due to the annealing process.

Acknowledgements

The authors gratefully acknowledge partial financial support from the UNC Charlotte Center for Precision Metrology Affiliates Program.

References

[1] Cooke, A.L. and Soons, J.A., 2010, Variability in the geometric accuracy of additively manufactured test parts, 21st Annual International Solid Freeform Fabrication Symposium, Austin, TX.

[2] Schmitz, T. and Smith, K.S., 2008, Machining Dynamics: Frequency Response to Improved Productivity, Springer, New York, NY.

[3] Rubeo, M. and Schmitz, T., 2016, Mechanistic force model coefficients: A comparison of linear regression and nonlinear optimization, Precision Engineering, 45: 311-321.

[4] Coelho, R.T., Braghini Jr., A., Valente, C.M.O. and Medalha, G.C., 2003, Experimental evaluation of cutting force parameters applying mechanistic model in orthogonal milling, Brazilian Society of Mechanical Science & Engineering, 247-248.

[5] Kienzle, O., 1952, Die Bestimmung von Kräften und Leistungen an spanenden Werkzeugen und Werkzeugmaschinen, In: Zeitschrift des Vereins deutscher Ingenieure, 657-662.